JOURNAL OF VIROLOGY, Oct. 2006, p. 9687–9696 Vol. 80, No. 19
0022-538X/06/$08.00+0 doi:10.1128/JVI.00738-06

Reduction of the Rate of Poliovirus Protein Synthesis through Large-Scale Codon Deoptimization Causes Attenuation of Viral Virulence by Lowering Specific Infectivity

Steffen Mueller,[1]* Dimitris Papamichail,[2] J. Robert Coleman,[1] Steven Skiena,[2] and Eckard Wimmer[1]

Department of Molecular Genetics and Microbiology[1] and Department of Computer Science,[2] Stony Brook University, Stony Brook, New York 11794

Received 11 April 2006/Accepted 18 July 2006

Exploring the utility of de novo gene synthesis with the aim of designing stably attenuated polioviruses (PV), we followed two strategies to construct PV variants containing synthetic replacements of the capsid coding sequences either by deoptimizing synonymous codon usage (PV-AB) or by maximizing synonymous codon position changes of the existing wild-type (wt) poliovirus codons (PV-SD). Despite 934 nucleotide changes in the capsid coding region, PV-SD RNA produced virus with wild-type characteristics. In contrast, no viable virus was recovered from PV-AB RNA carrying 680 silent mutations, due to a reduction of genome translation and replication below a critical level. After subcloning of smaller portions of the AB capsid coding sequence into the wt background, several viable viruses were obtained with a wide range of phenotypes corresponding to their efficiency of directing genome translation. Surprisingly, when inoculated with equal infectious doses (PFU), even the most replication-deficient viruses appeared to be as pathogenic in PV-sensitive CD155tg (transgenic) mice as the PV(M) wild type. However, infection with equal amounts of virus particles revealed a neuroattenuated phenotype over 100-fold. Direct analysis indicated a striking reduction of the specific infectivity of PV-AB-type virus particles. Due to the distribution effect of many silent mutations over large genome segments, codon-deoptimized viruses should have genetically stable phenotypes, and they may prove suitable as attenuated substrates for the production of poliovirus vaccines.

The rapidly developing technologies in the field of synthetic biology allow for the cost-efficient de novo synthesis of DNA sequences without the need for a natural template. This allows for the generation of entirely novel coding sequences or the modulation of existing sequences to a degree practically impossible with traditional cloning methods. Inspired by our previous work on the chemical synthesis of poliovirus (PV) in the absence of natural template (5), we are now actively exploring the utility of de novo gene synthesis for the customization of virus properties.

As a result of the degeneracy of the genetic code, all but two amino acids in the protein coding sequence can be encoded by more than one synonymous codon. The frequencies of synonymous codon use for each amino acid are unequal and have coevolved with the cell's translation machinery to avoid excessive use of suboptimal codons which often correspond to rare or otherwise disadvantaged tRNAs (10). This results in a phenomenon termed "synonymous codon bias," which varies greatly between evolutionarily distant species and possibly even between different tissues in the same species (24).

While codon optimization by recombinant methods (that is, to bring a gene's synonymous codon use into correspondence with the host cell's codon bias) has been widely used to improve cross-species expression (10), the opposite direction of reducing expression by intentional introduction of suboptimal synonymous codons has seldom been chosen.

In the present work, we have reengineered the capsid coding region of poliovirus type 1 Mahoney [PV(M)] by introducing through de novo gene synthesis the largest possible number of rarely used synonymous codons (PV-AB) or the largest possible codon position changes while maintaining the original codon bias (PV-SD). We found viruses arising from PV-AB-type designs to be attenuated by a previously underappreciated mechanism. While the primary defect of these genomes was at the level of genome translation, codon-deoptimized viruses were marked by a reduction in virus-particle-specific infectivity up to 1,000-fold. Thus, while producing similar amounts of virus particles per cell, production of infectious units (measured by functional assays) is greatly reduced. Due to the high degree of genetic stability as a result of the large number of mutations contributing to the phenotype, we propose that codon-deoptimized virus may present a useful and safer alternative for the production of poliovirus vaccines, especially inactivated vaccines.

At the time of submission of the manuscript for this article, a publication by Burns and colleagues appeared describing similar experiments with the Sabin type 2 vaccine strain of poliovirus (3). Our results largely agree with their findings, with the exception that we conclusively show genome translation to be the determinant of lower specific infectivity. Moreover, we have tested our novel strains in mice transgenic for the poliovirus receptor (CD155tg mice) for neurovirulence and found attenuation corresponding to the low infectious unit/particle ratio.

* Corresponding author. Mailing address: Department of Molecular Genetics and Microbiology, Life Sciences Building, Stony Brook University, Stony Brook, NY 11794-5222. Phone: (631) 632-8804. Fax: (631) 632-8891. E-mail: smueller@ms.cc.sunysb.edu.

MATERIALS AND METHODS

Cells, viruses, plasmids, and bacteria. HeLa R19 cell monolayers were maintained in Dulbecco's modified Eagle medium (DMEM) supplemented with 10% bovine calf serum (BCS) at 37°C. All PV infectious cDNA constructs are based

on PV1(M) cDNA clone pT7PVM (4, 33). Dicistronic reporter plasmids were constructed using pHRPF-Luc (35). *Escherichia coli* DH5α was used for plasmid transformation and propagation. Viruses were amplified by infection of HeLa R19 cell monolayers with 5 PFU per cell. Infected cells were incubated in DMEM (2% BCS) at 37°C until complete cytopathic effect (CPE) was apparent or for at least 4 days postinfection. After three rounds of freezing and thawing, the lysate was clarified of cell debris by low-speed centrifugation and the supernatant, containing the virus, was used for further passaging or analysis.

Cloning of synthetic capsid replacements and dicistronic reporter replicons. Two poliovirus genome cDNA fragments spanning the genome between nucleotides 495 and 3636, named SD and AB, were synthesized with the GeneMaker technology (Blue Heron Biotechnology; www.blueheronbio.com). pPV-SD and pPV-AB were generated by releasing the replacement cassettes from the vendor's cloning vector by PflMI digestion and insertion into the pT7PVM vector in which the corresponding PflMI fragment had been removed. pPV-AB$^{755–1513}$ and pPV-AB$^{2470–3386}$ were obtained by inserting a BsmI fragment or an NheI-EcoRI fragment, respectively, from pPV-AB into equally digested pT7PVM vector. In pPV-AB$^{1513–3386}$ and pPV-AB$^{755–2470}$, the BsmI fragment or NheI-EcoRI fragment of pT7PVM, respectively, replaces the respective fragment of the pPV-AB vector. Replacement of the NheI-EcoRI fragment of pPV-AB$^{1513–3386}$ with that of pT7PVM resulted in pPV-AB$^{2470–3386}$. Finally, replacement of the SnaBI-EcoRI fragments of pPV-AB$^{2470–3386}$ and pT7PVM with one another produced pPV-AB$^{2954–3386}$ and pPV-AB$^{2470–2954}$, respectively.

Cloning of dicistronic reporter constructs was accomplished by first introducing a silent mutation in pHRPF-Luc by site-directed mutagenesis using oligonucleotides Fluc-mutRI(+)/Fluc-mutRI(−) to mutate an EcoRI site in the firefly luciferase open reading frame and generate pdiLuc-mRI. The capsid regions of pT7PVM, pPV-AB$^{1513–2470}$, and pPV-AB$^{2470–2954}$ were PCR amplified using oligonucleotides RI-2A-P1wt(+)/P1wt-2A-RI(−). Capsid sequences of pPV-AB$^{2470–3386}$ and pPV-AB$^{2954–3386}$ or pPV-AB were amplified with RI-2A-P1wt(+)/P1AB-2A-RI(−) or RI-2A-P1AB(+)/P1AB-2A-RI(−), respectively. PCR products were digested with EcoRI and inserted into a now unique EcoRI site in pdiLuc-mRI to result in pdiLuc-PV, pdiLuc-AB$^{1513–2470}$, pdiLuc-AB$^{2470–2954}$, pdiLuc-AB$^{2470–3386}$, pdiLuc-AB$^{2954–3386}$, and pdiLuc-AB, respectively.

Oligonucleotides. The following oligonucleotides were used: Fluc-mutRI(+), 5′-GCACTGATAATGAACTCCTCTGGATCTACTGG-3′; Fluc-mutRI(−), 5′-CCAGTAGATCCAGAGGAGTTCATTATCAGTGC-3′; RI-2A-P1wt(+), 5′-CAAGAATTCCTGACCACATACGGTGCTCAGGTTTCATCACAGAAAGTGGG-3′; RI-2A-P1AB(+), 5′-CAAGAATTCCTGACCACATACGGTGCGCAAGTATCGTCGCAAAAAGTAGG-3; P1wt-2A-RI(−), 5′-TTCGAATTCTCCATATGTGGTCAGATCCTTGGTGGAGAGG-3′; and P1AB-2A-RI(−), 5′-TTCGAATTCTCCATACGTCGTTAAATCTTTCGTCGATAACG-3′.

In vitro transcription and RNA transfection. Driven by the T7 promoter, 2 μg of EcoRI-linearized plasmid DNA was transcribed by T7 RNA polymerase (Stratagene) for 1 h at 37°C. One microgram of virus or dicistronic transcript RNA was used to transfect 10^6 HeLa R19 cells on a 35-mm-diameter plate according to a modification of the DEAE-dextran method (33). Following a 30-min incubation at room temperature, the supernatant was removed and cells were incubated at 37°C in 2 ml of DMEM containing 2% BCS until CPE appeared, or the cells were frozen 4 days posttransfection for further passaging. Virus titers were determined by standard plaque assay on HeLa R19 cells using a semisolid overlay of 0.6% tragacanth gum (Sigma-Aldrich) in minimal Eagle medium.

In vitro and in vivo translations. Two different HeLa cell S10 cytoplasmic extracts were used in this study. A standard extract was prepared by the method of Molla et al. (19). [^{35}S]methionine-labeled translation products were analyzed by gel autoradiography. The second extract was prepared as described previously (17), except that it was not dialyzed and endogenous cellular mRNAs were not removed with micrococcal nuclease. Reactions with the modified extract were not supplemented with exogenous amino acids or tRNAs. Translation products were analyzed by Western blotting with anti-2C monoclonal antibody 91.23 (23). Relative intensities of 2BC bands were determined by a pixel count of the scanned gel image using the NIH-Image 1.62 software. In all cases, translation reactions were programmed with 200 ng of the various in vitro-transcribed viral genomic RNAs.

For analysis of in vivo translation, HeLa cells were transfected with in vitro-transcribed dicistronic replicon RNA as described above. In order to assess translation isolated from RNA replication, transfections were carried out in the presence of 2 mM guanidine hydrochloride. Cells were lysed after 7 h in passive lysis buffer (Promega) followed by a dual firefly (F-Luc) and *Renilla* (R-Luc) luciferase assay (Promega). Translation efficiency of the second cistron (P1-Fluc-P2-P3 polyprotein) was normalized through division by the *Renilla* luciferase activity of the first cistron expressed under control of the hepatitis C virus internal ribosome entry site (IRES).

Determination of virus titer by infected focus assay. Infections were done as for a standard plaque assay. After 48 or 72 h of incubation, the tragacanth gum overlay was removed and the wells were washed twice with phosphate-buffered saline (PBS) and fixed with cold methanol/acetone for 30 min. Wells were blocked in PBS containing 10% BCS followed by incubation with a 1:20 dilution of anti-3D mouse monoclonal antibody 125.2.3 (22) for 1 h at 37°C. After washing, cells were incubated with horseradish peroxidase-labeled goat anti-mouse antibody (Jackson ImmunoResearch) and infected cells were visualized using Vector VIP substrate kit (Vector Labs). Stained foci, which are equivalent to plaques obtained with wt virus, were counted, and titers were calculated as in the plaque assay procedure.

Molecular quantification of viral particles: direct OD_{260} absorbance method. Fifteen-centimeter dishes of HeLa cells (4×10^7 cells) were infected with PV(M), PV-AB$^{755–1513}$, or PV-AB$^{2470–2954}$ at a multiplicity of infection (MOI) of 0.5 until complete CPE occurred (overnight versus 4 days). Cell-associated virus was released by three successive freeze/thaw cycles. Cell lysates were cleared by 10 min of centrifugation at $2{,}000 \times g$ followed by a second 10-min centrifugation at $14{,}000 \times g$ for 10 min. Supernatants were incubated for 1 h at room temperature in the presence of 10 μg/ml RNase A (Roche) to digest any extraviral or cellular RNA. After addition of 0.5% sodium dodecyl sulfate (SDS) and 2 mM EDTA, virus-containing supernatants were overlaid on a 6-ml sucrose cushion (30% sucrose in Hanks balanced salt solution [HBSS]; Invitrogen). Virus particles were sedimented by ultracentrifugation for 4 h at 28,000 rpm using an SW28 swinging bucket rotor. Supernatants were discarded and centrifuge tubes were rinsed twice with HBSS while leaving the sucrose cushion intact. After removal of the last wash and the sucrose cushion, virus pellets were resuspended in PBS containing 0.2% SDS and 5 mM EDTA. Virus infectious titers were determined by plaque assay/infected-focus assay (see above). Virus particle concentrations were determined with a NanoDrop spectrophotometer (NanoDrop Technologies) at the optical density at 260 nm (OD_{260}) and calculated using the formula 1 OD_{260} unit = 9.4×10^{12} particles/ml (27). In addition, virion RNA was extracted by three rounds of phenol extraction and one round of chloroform extraction. RNA was ethanol precipitated and resuspended in ultrapure water. RNA purity was confirmed by TAE-buffered agarose gel analysis, and the concentration was determined spectrophotometrically. The total number of genome equivalents of the corresponding virus preparation was calculated via the determined RNA concentration and the molecular weight of the RNA. Thus, the relative amount of virions per infectious units could be calculated, assuming that 1 RNase-protected viral genome equivalent corresponds to 1 virus particle.

Molecular quantification of viral particles: ELISA method. Nunc Maxisorb 96-well plates were coated with 10 μg of rabbit anti PV1(M) (20) in 100 μl PBS for 2 h at 37°C and an additional 14 h at 4°C, and then the plates were washed three times briefly with 350 μl PBS and blocked with 350 μl of 10% bovine calf serum in PBS for 1 h at 37°C. Following three brief washes with PBS, wells were incubated with 100 μl of virus-containing cell lysates or controls in DMEM plus 2% BCS for 4 h at room temperature. Wells were washed with 350 μl PBS three times for 5 min each. Wells were then incubated for 4 h at room temperature with 2 μg of CD155-alkaline phosphatase (AP) fusion protein (11) in 100 μl DMEM–10% BCS. After the last of five washes with PBS,100 μl of 10 mM Tris, pH 7.5, was added and plates were incubated for 1 h at 65°C. Colorimetric alkaline phosphatase determination was accomplished by addition of 100 μl of 9 mg/ml *para*-nitrophenylphosphate (in 2 M diethanolamine, 1 mM $MgCl_2$, pH 9.8). Alkaline phosphatase activity was determined, and virus particle concentrations were calculated in an enzyme-linked immunosorbent assay (ELISA) plate reader (Molecular Devices) at a 405-nm wavelength on a standard curve prepared in parallel using twofold serial dilutions of a known concentration of purified PV(M) virus stock.

Mouse neuropathogenicity tests. Groups of four to five CD155tg mice (strain Tg21) (18) between 6 and 8 weeks of age were injected intracerebrally with virus dilutions between 10^2 and 10^6 PFU/focus-forming units (FFU) in 30 μl PBS. Fifty percent lethal dose (LD_{50}) values were calculated by the method of Reed and Muench (25). Virus titers in spinal cord tissues at the time of death or paralysis were determined by plaque or infected-focus assay. All experiments involving mice were conducted in compliance with institutional IACUC regulations and federal guidelines.

RESULTS

Design of codon-deoptimized polioviruses. We produced two different synonymous encodings of the poliovirus P1 capsid

region, each governed by different design criteria. We limited our designs to the capsid, as it has been conclusively shown that the entire capsid coding sequence can be deleted from the poliovirus genome or replaced with exogenous sequences without affecting replication of the resulting subgenomic replicon (15, 17). It is therefore quite certain that no unidentified crucial regulatory RNA elements are located in the capsid region, which might be affected inadvertently by modulation of the RNA sequence.

In the first design (PV-SD), we sought to maximize the number of RNA base changes while preserving the exact codon usage distribution of the wild-type P1 region (Fig. 1). To achieve this, we exchanged synonymous codon positions for each amino acid by finding a maximum weight bipartite match (8) between the positions and the codons, where the weight of each position-codon pair is the number of base changes between the original codon and the synonymous candidate codon to replace it. To avoid any positional bias from the matching algorithm, the synonymous codon locations were randomly permuted before creating the input graph and the locations were subsequently restored. We used Rothberg's maximum bipartite matching program (26) to compute the matching. A total of 11 useful restriction enzyme sites, each 6 nucleotides, were locked in the viral genome sequence so as to not participate in the codon location exchange. The codon shuffling technique potentially creates additional restriction sites that we prefer to remain unique in the resulting reconstituted full-length genome. For this reason, we further processed the sequence by substituting codons to eliminate the undesired sites. This resulted in an additional nine synonymous codon changes that slightly altered the codon frequency distribution. However, no codon had its frequency changed by more than 1 over the wild-type sequence. In total, there were 934 out of 2,643 nucleotides changed in the PV-SD capsid design when compared to the wild-type P1 sequence while maintaining the identical protein sequence of the capsid coding domain (Fig. 1 and see Fig. S1 posted at http://ms.cc.sunysb.edu/~smueller/FigureS1/FigureS1.html). As the codon usage was not changed, the GC content in the PVM-SD capsid coding sequence remained identical to that in the wt at 49%.

The second design, PV-AB, sought to drastically change the codon usage distribution over the wild-type P1 region. We were influenced by recent work suggesting codon bias may impact tissue-specific expression (24). Our desired codon usage distribution was derived from the most unfavorable codons observed in a previously described set of brain-specific genes (14, 24). We synthesized a capsid coding region maximizing the usage of the rarest synonymous codon for each particular amino acid as observed in this set of genes (Fig. 1). Since for all amino acids but one (leucine) the rarest codon in brain corresponds to the rarest codons among all human genes at large, in effect this design would be expected to discriminate against expression in other mammalian tissues as well. Altogether the PV-AB capsid differs from the wt capsid in 680 nucleotide positions (see Fig. S1 at http://ms.cc.sunysb.edu/~smueller/FigureS1/FigureS1.html). The GC content in the PVM-AB capsid region was reduced to 43% compared to 49% in the wt.

Codon-deoptimized polioviruses display severe growth phenotypes. Of the two initial capsid ORF replacement designs (Fig. 2A), only PV-SD produced viable virus. In contrast, no

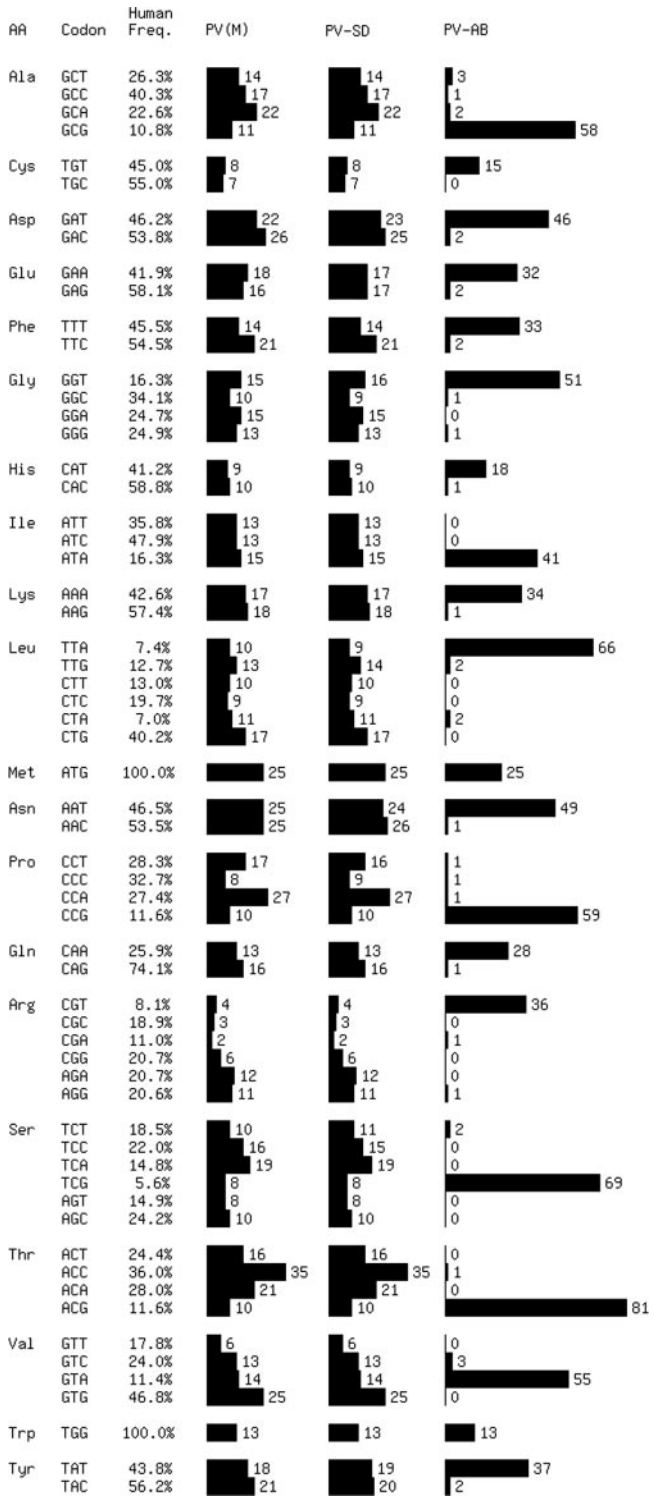

FIG. 1. Codon use statistics in synthetic P1 capsid designs. PV-SD maintains nearly identical codon frequencies compared to wt, while maximizing codon positional changes within the sequence. In PV-AB capsids, the use of nonpreferred codons was maximized. The lengths of the bars and the numbers behind each bar indicate the occurrence of each codon in the sequence. As a reference, the normal human synonymous codon frequencies(Freq. [as a percentage of 100]) for each amino acid are given in the third column.

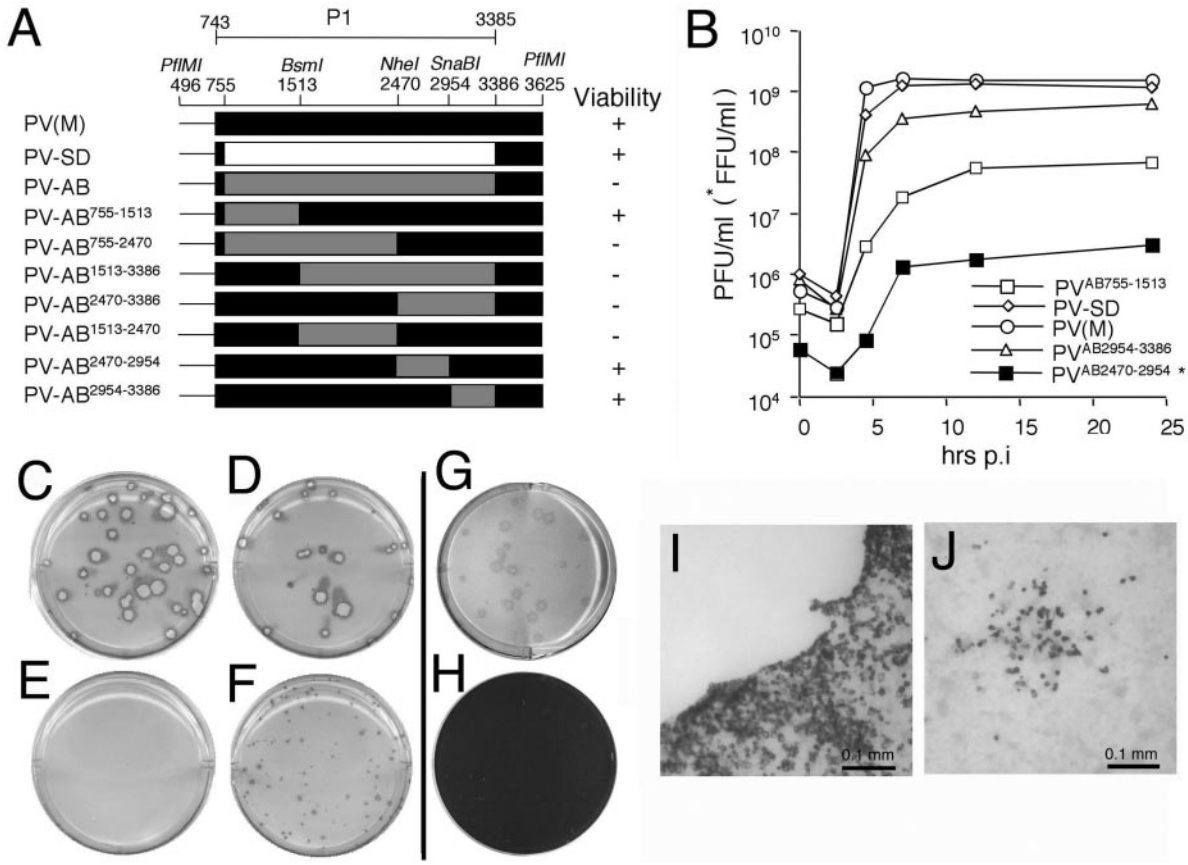

FIG. 2. Codon-deoptimized virus phenotypes. (A) Overview of virus constructs used in this study. (B) One-step growth kinetics in HeLa cell monolayers. (C to H) Plaque phenotypes of codon-deoptimized viruses after 48 h (C to F) or 72 h (G and H) of incubation; stained with anti $3D^{pol}$ antibody to visualize infected cells. (C) PV(M), (D) PV-SD, (E) PV-AB, (F) PV-$AB^{755–1513}$, (G and H) PV-$AB^{2470–2954}$. Cleared plaque areas are outlined by a rim of infected cells (C and D). (H) No plaques are apparent with PV-$AB^{2470–2954}$ after subsequent crystal violet staining of the well shown in panel G. (I and J) Microphotographs of the edge of an immunostained plaque produced by PV(M) (I) or an infected focus produced by PV-$AB^{2470–2954}$ (J) after 48 h of infection.

viable virus was recovered from four independent transfections with PV-AB RNA, even after three rounds of passaging (Fig. 2E). It appeared that the codon bias we introduced into the PV-AB genome was too severe. Thus, we subcloned smaller portions of the PV-AB capsid coding sequence into the PV(M) background to reduce the detrimental effects of the nonpreferred codons. Of these subclones, PV-$AB^{2954–3386}$ produced cytopathic effect 40 h after RNA transfection, while PV-$AB^{755–1513}$ and PV-$AB^{2470–2954}$ required one or two additional passages following transfection, respectively (compared to 24 h for the wt virus). Interestingly, they represent the three subclones with the smallest portions of the original AB sequence, an observation suggesting a direct correlation between the number of nonpreferred codons and the fitness of the virus.

One-step growth kinetics of all viable virus variants were determined by infecting HeLa monolayers at an MOI of 2 with viral cell lysates obtained after a maximum of two passages following RNA transfection (Fig. 2B). The MOI was chosen due to the low titer of PV-$AB^{2470–2954}$ and to eliminate the need for further passaging required for concentrating and purifying the inoculum. Under the conditions used, all viruses had produced complete or near complete CPE by 24 h postinfection.

Despite 934 single-point mutations in its capsid region, PV-SD replicated at wild-type capacity (Fig. 2B) and produced similarly sized plaques as the wild type (Fig. 2D). While PV-$AB^{2954–3386}$ grew with near-wt kinetics (Fig. 2B), PV-$AB^{755–1513}$ produced minute plaques and approximately 22-fold less infectious virus (Fig. 2B and F, respectively). Although able to cause CPE in high-MOI infections, albeit much delayed (80 to 90% CPE after 20 to 24 h), PV-$AB^{2470–2954}$ produced no plaques at all under the conditions of the standard plaque assay (Fig. 2H). We therefore quantified this virus using a focus-forming assay, in which foci of infected cells after 72 h of incubation under plaque assay conditions were counted after they were stained immunohistochemically with antibodies to the viral polymerase 3D (Fig. 2G). After 48 h of infection, PV-$AB^{2470–2954}$-infected foci usually involved only tens to hundreds of cells (Fig. 2J) with a focus diameter of 0.2 to 0.5 mm, compared to 3-mm plaques for the wt (Fig. 2C and I). However, after an additional 24 h, the diameter of the foci increased significantly (2 to 3 mm; Fig. 2G). When HeLa cells were infected with PV-$AB^{755–1513}$ and PV-$AB^{2470–2954}$ at an MOI of 1, the CPE appeared between 12 and 18 h and 3 and 4 days, respectively, compared to 8 h with the wt (data not shown).

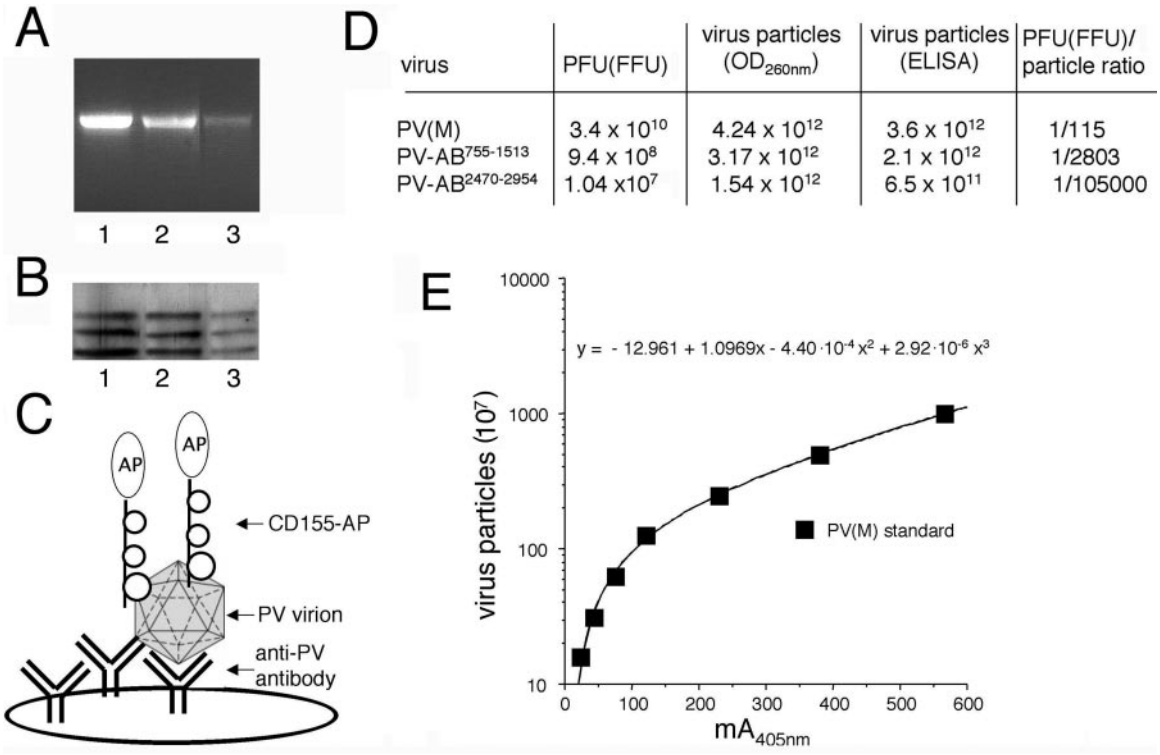

virus	PFU(FFU)	virus particles (OD_{260nm})	virus particles (ELISA)	PFU(FFU)/ particle ratio
PV(M)	3.4×10^{10}	4.24×10^{12}	3.6×10^{12}	1/115
PV-AB$^{755\text{-}1513}$	9.4×10^{8}	3.17×10^{12}	2.1×10^{12}	1/2803
PV-AB$^{2470\text{-}2954}$	1.04×10^{7}	1.54×10^{12}	6.5×10^{11}	1/105000

FIG. 3. Codon deoptimization leads to a reduction of specific infectivity. (A) Agarose gel electrophoresis of virion genomic RNA isolated from purified virus particles of PV(M) (lane 1), PV-AB$^{755–1513}$ (lane 2), and PV-AB$^{2470–2954}$ (lane 3). (B) Silver-stained SDS-PAGE protein gel of purified PV(M) (lane 1), PV-AB$^{755–1513}$ (lane 2), and PV-AB$^{2470–2954}$ (lane 3) virus particles. The three larger of the four capsid capsid proteins (VP1, VP2, and VP3) are shown, demonstrating the purity and relative amounts of virus preparations. (C) Development of a virus capture ELISA using a poliovirus receptor-alkaline phosphatase (CD155-AP) fusion protein probe. Virus-specific antibodies were used to coat ELISA plates, and samples containing an unknown virus concentration were applied followed by detection with CD155-AP. Virus concentrations were calculated using a standard curve prepared in parallel with known amounts of purified wt virus (E). (D) The amounts of purified virus and extracted virion RNA were spectrophotometrically quantified, and the number of particles or genome equivalents (1 genome = 1 virion) was calculated. In addition, virion concentrations were determined by ELISA. The infectious titer of each virus was determined by plaque/infected-focus assay, and the specific infectivity was calculated as PFU/particle or FFU/particle.

In order to quantify the cumulative effect of a particular codon bias in a protein coding sequence, we calculated a relative codon deoptimization index (RCDI), which is a comparative measure against the general codon distribution in the human genome. An RCDI = 1/codon indicates that a gene follows the normal human codon frequencies, while any deviation from the normal human codon bias results in an RCDI higher than 1. We derived the RCDI by the formula $RCDI = [\Sigma(C_iF_a/C_iF_h) \cdot N_{Ci}]/N(i = 1 \text{ through } 64)$.

C_iF_a is the observed relative frequency in the test sequence of each codon i out of all synonymous codons for the same amino acid (0 to 1), C_iF_h is the normal relative frequency observed in the human genome of each codon i out of all synonymous codons for that amino acid (0.06 to 1), N_{Ci} is the number of occurrences of that codon i in the sequence, and N is the total number of codons (amino acids) in the sequence.

Thus, a high number of rare codons in a sequence results in a higher index. According to this formula, we calculated RCDI values of the various capsid coding sequences of 1.14 for PV(M) and PV-SD which is very close to a normal human distribution. The RCDI values for the AB constructs are 1.73 for PV-AB$^{755–1513}$, 1.45 for PV-AB$^{2470–2954}$, and 6.51 for the parental PV-AB.

For comparison, the RCDI for probably the best known codon-optimized protein, "humanized" green fluorescent protein (GFP), was 1.31 compared to an RCDI of 1.68 for the original *Aequora victoria gfp* gene (36). According to these calculations, a capsid coding sequence with an RCDI of <2 is associated with a viable virus phenotype, while an RCDI of >2 (PV-AB = 6.51, PV-AB$^{1513–3386}$ = 4.04, PV-AB$^{755–2470}$ = 3.61) would result in a lethal phenotype.

The PFU/particle ratio is reduced in codon-deoptimized viruses. The extremely poor growth phenotype of PV-AB$^{2470–2954}$ in cell culture and its inability to form plaques suggested a defect in cell-to-cell spreading that may be consistent with a lower specific infectivity of the individual virus particles.

To test this hypothesis, we purified PV(M), PV-AB$^{755–1513}$, and PV-AB$^{2470–2954}$ virus and determined the amount of virus particles spectrophotometrically. Purified virus preparations were quantified directly by measuring the OD_{260}, and particle concentrations were calculated according to the formula 1 OD_{260} unit = 9.4×10^{12} particles/ml (Fig. 3D) (27). Additionally, genomic RNA was extracted from those virions (Fig. 3A) and quantified at OD_{260} (data not shown). The number of virions (1 virion = 1 genome) was then determined via the molecular size of 2.53×10^6 g/mol for genomic RNA. Specif-

ically, virus was prepared from 4×10^7 HeLa cells that were infected with 0.5 MOI of virus until the appearance of complete CPE, as described in Materials and Methods. Both methods of particle determinations produced similar results (Fig. 3D). Indeed, it was found that PV(M) and PV-AB$^{755–1513}$ produced roughly equal amounts of virions, while PV-AB$^{2470–2954}$ produced between 1/3 (by the direct UV method (Fig. 3D) to 1/8 of the number of virions compared to PV(M) (by RNA genome method [data not shown]). In contrast, the wt virus sample corresponded to approximately 30 times and 3,000 times more infectious units than PV-AB$^{755–1513}$ and PV-AB$^{2470–2954}$, respectively (Fig. 3D). In addition, capsid proteins of purified virions were resolved by SDS-polyacrylamide gel electrophoresis (PAGE) and visualized by silver staining (Fig. 3B). These data as well support the conclusion that on a per-cell basis, PV-AB$^{2470–2954}$ and PV-AB$^{755–1513}$ produce similar or only slightly reduced amounts of progeny per cell (Fig. 3B, lane 3), while their PFU/particle ratio is reduced. The PFU/particle ratio for a virus can vary significantly depending on the methods to determine either plaques (cell type for plaque assay and the particular plaque assay technique) or particle count (spectrophotometry or electron microscopy). By our method, we determined a PFU/particle ratio for PV1(M) of 1/115, which compares well to previous determinations of 1/272 (16) (done on HeLa cells) and 1/87 (29) (in primary monkey kidney cells).

Development of a virion-specific ELISA. To confirm the reduced PFU/particle ratio observed with codon-deoptimized PVs, we developed a novel virion-specific ELISA (Fig. 3C and E) as a way to determine the physical amount of intact viral particles in a sample rather than the infectious titer, which is a biological variable. The assay is based on our previous observation that the ectodomain of the poliovirus receptor CD155 fused to heat-stable placental alkaline phosphatase (CD155-AP) binds very tightly and specifically to the intact 160S particle (11). Considering that poliovirus 130S particles (A particles) lose their ability to bind CD155 efficiently (12), it can be expected that neither any other capsid intermediate nor capsid subunits should interact with CD155-AP, thus ensuring specificity for intact particles. In support of this notion, lysates from cells that were infected with a vaccinia virus strain expressing the P1 capsid precursor (1), resulted in no quantifiable signal (data not shown).

The ELISA method allows for the quantification of virus particles in a crude sample such as the cell lysate after infection, which should minimize possible alteration of the PFU/particle ratio by other mechanisms during sample handling and purification (thermal/chemical inactivation, oxidation, degradation, etc.). Under the current conditions, the sensitivity of this assay is approximately 10^7 viral particles, as there is no signal amplification step involved. This, in turn, resulted in an exceptionally low background. With this ELISA, we were able to determine PV particle concentrations in our samples by back calculation on a standard curve prepared with purified PV(M) of known concentration (Fig. 3E). The particle determinations by ELISA agreed well with results obtained by the direct UV method (Fig. 3D).

Codon-deoptimized polioviruses are neuroattenuated on a particle basis in CD155tg mice. To test the pathogenic potential of viruses constructed in this study, we injected CD155 transgenic mice (18) intracerebrally with PV(M), PV-SD and PV-AB$^{755–1513}$, and PV-AB$^{2470–2954}$ at doses between 10^2 and 10^5 PFU/FFU.

TABLE 1. Neuropathogenicity in CD155tg mice

Construct	LD_{50}		Spinal cord titer	
	PFU or FFU[a]	No. of virions[b]	PFU or FFU/g[c]	No. of virions/g[d]
PV(M) wt	3.2×10^2 PFU	3.7×10^4	1.0×10^9 PFU	1.15×10^{11}
PV$^{AB755–1515}$	2.6×10^2 PFU	7.3×10^5	3.5×10^7 PFU	9.8×10^{10}
PV$^{AB2470–2954}$	4.6×10^1 FFU	4.8×10^6	3.4×10^6 FFU	3.57×10^{11}

[a] LD_{50} expressed as the number of infectious units, as determined by plaque or infectious focus assay, required to result in 50% lethality after intracerebral inoculation.
[b] LD_{50} expressed as the number of virus particles, as determined by OD_{260} measurement, required to result in 50% lethality after intracerebral inoculation.
[c] Virus recovered from the spinal cord of infected mice at the time of death or paralysis; expressed in PFU or FFU/g of tissue, as determined by plaque or infectious focus assay.
[d] Virus recovered from the spinal cord of infected mice at the time of death or paralysis, expressed in particles/g of tissue, derived by multiplying values in the third column by the particle/PFU ratio characteristic for each virus (Fig. 3D).

Our initial results were perplexing, as quite counterintuitively PV-AB$^{755–1513}$ and especially PV-AB$^{2470–2954}$ were found to be as neuropathogenic as or even slightly more neuropathogenic than the wt virus (Table 1). In addition, times of onset of paralysis following infection with PV-AB$^{755–1513}$ and PV-AB$^{2470–2954}$ were comparable to that of wt virus (data not shown). Similarly confounding was our observation that at time of death or paralysis, the viral loads, as determined by plaque assay, in the spinal cords of mice infected with PV-AB$^{755–1513}$ and PV-AB$^{2470–2954}$ were 30- and 300-fold lower, respectively, than those in the mice infected with the wt virus (Table 1). Thus, it seemed unlikely that PV-AB$^{2470–2954}$, apparently replicating at only 0.3% of the wt virus, would have the same neuropathogenic potential as the wt. However, after having established the altered PFU/particle relationship in PV-AB$^{755–1513}$ and PV-AB$^{2470–2954}$ (see above), we were now able to correlate the amount of inocculum with the actual number of particles inoculated. After performing this correction, we established that on a particle basis, PV-AB$^{755–1513}$ and PV-AB$^{2470–2954}$ are 20-fold and 100-fold neuroattenuated, respectively, compared to the wt (Table 1). Furthermore, on a particle basis the viral loads in the spinal cords of paralyzed mice were very similar with all three viruses (Table 1).

Codon-deoptimized viruses are deficient at the level of genome translation. Since our synthetic viruses and the wt PV(M) are indistinguishable in their protein makeup and no known RNA-based regulatory elements were altered in the modified RNA genomes, these designs allowed us to study the effect of reduced genome translation/replication on attenuation without affecting cell and tissue tropism or immunological properties of the virus. The PV-AB genome was designed under the hypothesis that introduction of many suboptimal codons into the capsid coding sequence should lead to a reduction of genome translation. Since the P1 region is at the N terminus of the polyprotein, synthesis of all downstream nonstructural proteins is determined by the rate of translation through the P1 region. To test whether in fact translation is affected, in vitro translations were performed (Fig. 4). Unex-

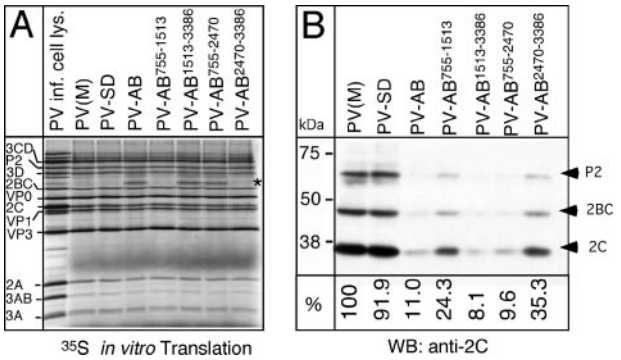

FIG. 4. The PV-AB phenotype is determined at the level of genome translation. (A) A standard in vitro translation in HeLa S10 extract, in the presence of exogenously added amino acids and tRNAs reveals no differences in translation capacities of codon-deoptimized genomes compared to the PV(M) wt. Shown is an autoradiograph of [^{35}S]methionine-labeled translation products resolved on a 12.5% SDS-PAGE gel. The identity of an aberrant band (*) is not known. (B) In vitro translation in nondialyzed HeLa S10 extract without the addition of exogenous amino acids and tRNA and in the presence of competing cellular mRNAs uncovers a defect in translation capacities of codon-deoptimized PV genomes. Shown is a Western blot of poliovirus 2C reactive translation products (2C^{ATPase}, 2BC, and P2) resolved on a 10% SDS-PAGE gel. The relative amounts of the 2BC translation products are expressed below each lane as percentages of the wt band.

pectedly, our initial translations in a standard HeLa-cell based cytoplasmic S10 extract (19) showed no difference in translation capacities for any of the genomes tested (Fig. 4A). However, as this translation system is optimized for maximal translation, it includes the exogenous addition of excess amino acids and tRNAs, which could conceivably compensate for the genetically engineered codon bias. Therefore, we repeated in vitro translations with a modified HeLa cell extract, which was not dialyzed and in which cellular mRNAs were not removed by micrococcal nuclease treatment (Fig. 4B). Translations in this extract were performed without the addition of exogenous tRNAs or amino acids. Thus, an environment was created that more closely resembles that in the infected cell, where translation of the PV genomes relies only on cellular supplies while competing for resources with cellular mRNAs. Due to the high background translation from cellular mRNA and the low [^{35}S]Met incorporation rate in nondialyzed extract, a set of virus-specific translation products were detected by Western blotting with anti-2C antibodies (23). These modified conditions resulted in dramatic reduction of translation efficiencies of the modified genomes which correlated with the extent of the deoptimized sequence. Whereas translation of PV-SD was comparable to that of the wt, translation of three noninfectious genomes, PV-AB, PV-AB$^{1513–3386}$, and PV-AB$^{755–2470}$, was reduced by approximately 90% (Fig. 4B).

Considering the ultimately artificial nature of the in vitro translation system, we sought to determine the effect of various capsid designs on translation in cells. For this purpose, dicistronic poliovirus reporter replicons were constructed (Fig. 5A) which are based on our previously reported dicistronic replicon (35). Various P1 cassettes were inserted immediately upstream and in-frame with the firefly luciferase (F-Luc) gene. Thus, the poliovirus IRES drives expression of a single viral polyprotein similar to the one in the viral genome, with the exception of the firefly luciferase protein between the capsid and the 2A^{pro} proteinase. Expression of the *Renilla* luciferase (R-Luc) gene under the control of the hepatitis C virus IRES provides an internal control. All experiments were carried out in the pres-

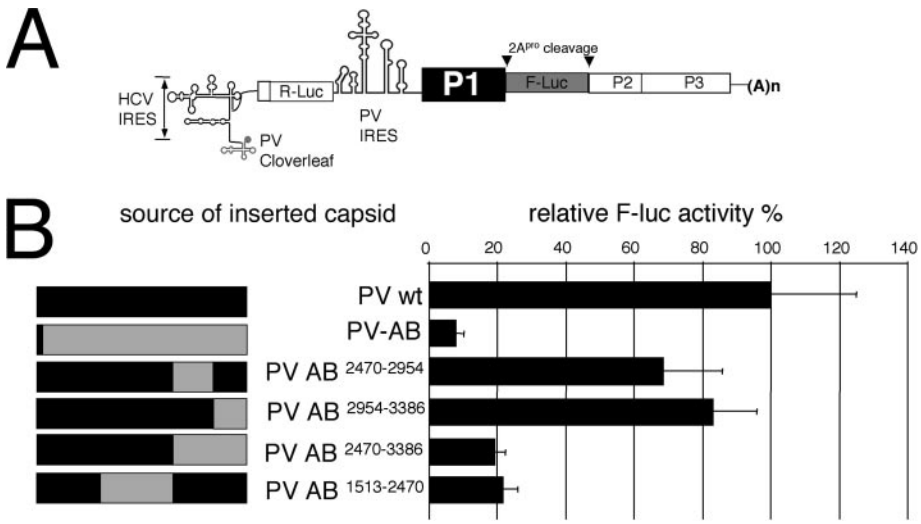

FIG. 5. Analysis of in vivo translation using dicistronic reporter replicons confirms the detrimental effect of codon deoptimization on PV translation. (A) Schematic of dicistronic replicons. Various P1 capsid coding sequences were inserted upstream of the firefly luciferase gene (F-Luc). Determination of changing levels of F-Luc expression relative to an internal control (R-Luc) allows for the quantification of ribosome transit through the P1 capsid region. (B) Replicon RNAs were transfected into HeLa cells and incubated for 7 h in the presence of 2 mM guanidine-hydrochloride to block RNA replication. The relative rate of translation through the P1 region was inversely proportional to the extent of codon deoptimization. While the capsid coding sequences of two viable virus constructs, PV-AB$^{2470–2954}$ and PV-AB$^{2954–3386}$, allow between 60 and 80% of wt translation, translation efficiency below 20% is associated with the lethal phenotypes observed with the PV-AB, PV-AB$^{2470–3386}$, and PV-AB$^{1513–2470}$ genomes. Each value represents the average of six determinations from three independent experiments.

ence of 2 mM guanidine hydrochloride, which completely blocks genome replication (34). Using this type of construct allowed an accurate determination of the relative expression of the second cistron by calculating the F-Luc/R-Luc ratio. As F-Luc expression depends on successful transit of the ribosome through the upstream P1 region, it provides a measure of the effect of the inserted P1 sequence on the rate of polyprotein translation. Using this method, we found indeed that the modified capsid coding regions, which were associated with a lethal phenotype in the virus background (e.g., PV-AB, PV-AB$^{1513–2470}$, and PV-AB$^{2470–3386}$) reduced the rate of translation by approximately 80 to 90% (Fig. 5B). Capsids from two viable virus constructs, PV-AB$^{2470–2954}$ and PV-AB$^{2954–3386}$, allowed translation at 68% and 83% of wt levels, respectively. In vivo translation rates of the first cistron remained constant in all constructs over a time period between 3 and 12 h, suggesting that RNA stability is not affected by the codon alterations (data not shown). In conclusion, the results of these experiments suggest that poliovirus is extremely dependent on very efficient translation as a relatively small drop in translation efficiency through the P1 region of 30%, as seen in PV-AB$^{2470–2954}$, resulted in a severe virus replication phenotype.

DISCUSSION

In the present work, we have demonstrated the utility of large-scale codon deoptimization of poliovirus capsid coding sequences by de novo gene synthesis for the generation of attenuated viruses. It was our initial goal to explore the potential of this technology as a tool for generating live attenuated virus vaccines. However, we found codon-deoptimized viruses to be marked by a very low specific infectivity (Fig. 3). In addition, our intention to design PV capsid encoding with a synonymous codon bias that specifically discriminated against expression in the central nervous system did not bear fruit, as the tissue-specific differences in codon bias described by others (24), if at all significant, are too small to bring about a tissue-restrictive virus phenotype. In a larger set of brain-specific genes than the one used by Plotkin and colleagues (24) in their calculations, we could not detect any appreciable tissue-specific codon bias (data not shown). These observations may pose hurdles to using this new technology to develop codon-deoptimized viruses as candidates for live attenuated vaccines, although much more work has to be carried out. Fine-tuning of codon deoptimization may still allow the alteration of tissue tropism and virulence required for attenuation.

On the other hand, codon-deoptimized viruses produced similar amounts of progeny per cell, while being 2 to 3 orders of magnitude less infectious (Fig. 3 and Table 1). Such viruses may prove very useful as safer alternatives in the production of inactivated poliovirus vaccine. Since they are 100% identical to the wt virus at the protein level, an identical immune response in hosts who received inactivated virus is guaranteed. This may be of great advantage at the stage of licensing any potential vaccine based on this strategy. Due to the distribution effect of many silent mutations over large genome segments, codon-deoptimized viruses should prove extremely genetically stable. Although long-term passaging experiments are still under way, no faster-replicating escape variants have been isolated from either PV-AB$^{2470–2954}$ or PV-AB$^{755–1513}$ after five passages, as assessed by the absence of faster-growing or large-plaque revertants (data not shown).

In addition, large-scale codon deoptimization of the poliovirus capsid coding region revealed interesting insights into the biology of the poliovirus itself. What determines the PFU/particle ratio (specific infectivity) of a virus has been a long-standing question. In general, failure at any step during the infectious life cycle before the establishment of a productive infection will lead to an abortive infection and, therefore, to the demise of the infecting particle. In the case of poliovirus, it has been shown that approximately 100 virions are required to result in one infectious event in cultured cells (16, 29). That is, of 100 particles inoculated, only a fraction are likely to succeed at the level of (step 1) receptor binding, followed by (step 2) internalization and uncoating, (step 3) initiation of genome translation, (step 4) polyprotein translation, (step 5) RNA replication, and (step 6) encapsidation of progeny.

In the infectious cycle of AB-type viruses described here, steps 1 and 2 should be identical to a PV(M) infection as their capsids are identical. Likewise, identical 5′ nontranslated regions should perform equally well in assembly of a translation complex (step 3). Viral polyprotein translation, on the other hand (step 4), is severely debilitated due to the introduction of a great number of suboptimal synonymous codons in the capsid region (Fig. 4 and 5). It is thought that the repeated encounter of rare codons by the translational machinery causes stalling of the ribosome as by the laws of mass action rare aminoacyl-tRNA will take longer to diffuse into the A site on the ribosome. As peptide elongation to a large extent is driven by the concentration of available aminoacyl-tRNA, dependence of an mRNA on many rare tRNAs, consequently, lengthens the time of translation (10). Alternatively, excessive stalling of the ribosome may cause premature dissociation of the translation complex from the RNA and result in a truncated protein destined for degradation. Both processes lead to a lower protein synthesis rate per mRNA molecule per unit of time. While our data presented here suggest that the phenotypes of codon-deoptimized viruses are determined by the rate of genome translation, other mechanistic explanations may be possible. It has been suggested that the conserved positions of rare synonymous codons throughout the viral capsid sequence in hepatitis A virus are of functional importance for the proper folding of the nascent polypeptide by introducing necessary translation pauses (28). Large-scale alteration of the codon composition may therefore conceivably change some of these pause sites to result in an increase of misfolded capsid proteins. Whether these considerations also apply to the PV capsid is not clear. If so, we would have expected a phenotype with our PV-SD design, in which the wt codons were preserved but their positions throughout the capsid were completely changed: that is, none of the purported pause sites would be at the appropriate position with respect to the protein sequence. No phenotype, however, was observed and PV-SD translated and replicated at wt levels (Fig. 2B). Another possibility is that the large-scale codon alterations in our designs may create fortuitous dominant-negative RNA elements, such as stable secondary structures, or sequences that may undergo disruptive long-range interactions with other regions of the genome.

We assume that all steps prior to, and including, virus uncoating should be unchanged when wt and our mutant viruses,

described here, are compared. This is supported by the observation that the eclipse period for all these isolates is similar (Fig. 2B). The dramatic reduction in PFU/particle ratio is, therefore, likely to be a result of the reduced translation capacity of the deoptimized genomes. That is, the handicap of the mutant viruses is determined intracellularly. It is generally assumed that the relatively low PFU/particle ratio of picornaviruses of 1/100 to 1/1,000 (27) is mainly determined by structural alterations at the receptor binding step, either prior to or at the level of cell entry. The formation of 135S particles that are hardly infectious may be the major culprit behind the inefficiency of poliovirus infectivity (12). However, certain virus mutants seem to sidestep A particle conversion without resulting in a higher specific infectivity, an observation suggesting that other postentry mechanisms may be responsible for the low PFU/particle ratio (7). Our data present clear evidence for such postentry interactions between virus and cell and that these events contribute to the distinct PFU/particle ratio of poliovirus. As all replication proteins are located downstream of P1 on the polyprotein, they critically depend upon successful completion of P1 translation. Lowering the rate of P1 translation therefore lowers translation of all replication proteins to the same extent. This, in turn, likely leads to a reduced capacity of the virus to make the necessary modifications to the host cell required for establishment of a productive infection, such as shutdown of host cell translation or prevention of host cell innate responses. While codon deoptimization, as described here, is likely to affect translation at the peptide elongation step, reduced initiation of translation can be a powerful attenuating determinant as well, as has been shown for mutations in the internal ribosomal entry site in the Sabin vaccine strains of poliovirus (30, 31).

On the basis of these considerations, we predict that many mutant phenotypes attributable to defects in genome translation or early genome replication actually manifest themselves by lowering PFU/particle ratios. This would be the case as long as the defect results in an increased chance of abortive infection. Since in almost all studies the omnipresent plaque assay is the virus detection method of choice, a reduction in the apparent virus titer is often equated with a reduction in virus production per se. This may be an inherent pitfall that can be excused with the difficulties of characterizing virus properties at the single-cell level. Instead, most assays are done on a large population of cells. A lower readout of the chosen test (protein synthesis, RNA replication, virus production as measured in PFU) is taken at face value as an indicator of lower production on a per-cell basis, without considering that virus production in a cell may be normal while the number of cells producing virus is reduced.

The near-identical production of particles per cell by codon-deoptimized viruses indicates that the total of protein produced after extended period of times is not severely affected, whereas the rate of protein production has been drastically reduced. This is reflected in the delayed appearance of CPE, which may be a sign that the virus has to go through more RNA replication cycles to build up similar intracellular virus protein concentrations. It appears that codon-deoptimized viruses are severely handicapped in establishing a productive infection because the early translation rate of the incoming infecting genome is reduced. As a result of this lower translation rate, poliovirus proteins essential for disabling the cell's antiviral responses (most likely proteinases $2A^{pro}$ and $3C^{pro}$) are not synthesized at sufficient amounts to pass this crucial hurdle in the life cycle quickly enough. Consequently, there is a better chance for the cell to eliminate the infection before viral replication could unfold and take over the cell. Thus, the chance for productive infection events is reduced and the rate of abortive infection is increased. However, in the case where a codon-deoptimized virus does succeed in disabling the cell, this virus will produce nearly identical amounts of progeny to the wild type. Our data suggest that a fundamental difference may exist between early translation (from the incoming RNA genome) and late translation during the replicative phase, when the cell's own translation is largely shut down. Although this may be a general phenomenon, it might be especially important in the case of codon-deoptimized genomes. Host cell shutoff very likely results in an overabundance of free aminoacyl-tRNAs which may overcome the imposed effect of the suboptimal codon usage as the PV genomes no longer have to compete with cellular RNAs for translation resources. This, in fact, may be analogous to our observations with the modified in vitro translation system described above (Fig. 4B). Here, in the translation extract, which was not nuclease treated (and thus contained the cellular mRNAs) and was not supplemented with exogenous amino acids or tRNA, clear differences were observed in the translation capacity of different capsid design mutants. Under these conditions, viral genomes have to compete with cellular mRNAs in an environment where supplies are limited. On the other hand, in the traditional translation extract, in which endogenous mRNAs were removed and tRNAs and amino acids were supplemented in excess, all PV RNAs translated equally well regardless of codon bias (Fig. 4A). These two different in vitro conditions may be analogous to in vivo translation during the early and late phases in the PV-infected cell.

One key finding of the present work is the realization that, besides the steps during the physical interaction and uptake of virus, the PFU/particle ratio is also to a great extent a result of the virus' capacity to overcome host cell antiviral responses. This suggests that picornaviruses are actually quite inefficient in winning this struggle. Rather they have taken the path of evolving small genomes that are quick enough to replicate before the cell can effectively respond. As our data show, slowing down translation rates by only 30% in PV-$AB^{2470–2954}$ (Fig. 5) leads to a 1,000-fold-higher rate of abortive infection as reflected in the lower specific infectivity (Fig. 3D). Picornaviruses apparently not only replicate at the threshold of error catastrophe (6, 13) but also at the threshold of elimination by the host cell's antiviral defenses. This effect may have profound consequences for the pathogenic phenotype of a picornavirus. We can at this point only speculate which cellular antiviral processes may be responsible for the increased rate of aborted infections by codon-deoptimized viruses. Poliovirus has been shown to both induce and inhibit apoptosis (2, 9, 32). Similarly poliovirus interfers with the interferon pathway by cleaving NF-κB (21). It is plausible that a PV with a reduced rate of early genome translation still induces antiviral responses in the same way as a wt virus (induction of apoptosis and interferon by default) but then, due to the low protein synthesis, has a reduced potential of inhibiting these processes. Such a scenario

would reasonably increase the chances of the cell to abort a starting infection and could explain the phenomena observed here.

At the individual cell level, poliovirus infection is likely to be an all-or-nothing phenomenon. Viral protein and RNA syntheses likely need to be within a very close to maximal range in order to ensure productive infection.

At the time of submission of the manuscript for this article, the work by Burns et al. appeared in which experiments related to our experiments were described (3). These authors did not alter codon usage to such a drastic extent as we did, and none of their mutant viruses expressed a lethal phenotype. Interestingly, Burns et al. described that translation did not play a major role in the altered phenotypes of their mutant viruses, a conclusion at variance with our data. Although our mutant viruses are quite different from theirs, we suggest that the assay used in their study explains their failure to detect drastic effects in translation. The effect of the mutations introduced by Burns and colleagues on mouse neurovirulence was not tested.

Since the dramatic effect of codon bias on poliovirus fitness could not be predicted, it should be possible in future designs to make less severe codon changes distributed over a larger number of codon sequences. This should continue to improve the genetic stability of the individual phenotypes and improve their potential as vaccine candidates.

ACKNOWLEDGMENTS

The authors would like to thank David Franco for assistance with the preparation of HeLa cell translation extracts and JoAnn Mugavero for technical help.

This work was supported by NIH grant AI15122 to E.W. and NSF grant EIA0325123 to S.S. S.M. was supported by NCI training grant T32-CA009176.

REFERENCES

1. **Ansardi, D. C., D. C. Porter, and C. D. Morrow.** 1993. Complementation of a poliovirus defective genome by a recombinant vaccinia virus which provides poliovirus P1 capsid precursor in *trans*. J. Virol. **67:**3684–3690.
2. **Belov, G. A., L. I. Romanova, E. A. Tolskaya, M. S. Kolesnikova, Y. A. Lazebnik, and V. I. Agol.** 2003. The major apoptotic pathway activated and suppressed by poliovirus. J. Virol. **77:**45–56.
3. **Burns, C. C., J. Shaw, R. Campagnoli, J. Jorba, A. Vincent, J. Quay, and O. Kew.** 2006. Modulation of poliovirus replicative fitness in HeLa cells by deoptimization of synonymous codon usage in the capsid region. J. Virol. **80:**3259–3272.
4. **Cao, X., R. J. Kuhn, and E. Wimmer.** 1993. Replication of poliovirus RNA containing two VPg coding sequences leads to a specific deletion event. J. Virol. **67:**5572–5578.
5. **Cello, J., A. V. Paul, and E. Wimmer.** 2002. Chemical synthesis of poliovirus cDNA: generation of infectious virus in the absence of natural template. Science **297:**1016–1018.
6. **Crotty, S., C. E. Cameron, and R. Andino.** 2001. RNA virus error catastrophe: direct molecular test by using ribavirin. Proc. Natl. Acad. Sci. USA **98:**6895–6900.
7. **Dove, A. W., and V. R. Racaniello.** 1997. Cold-adapted poliovirus mutants bypass a postentry replication block. J. Virol. **71:**4728–4735.
8. **Gabow, H.** 1973. Ph.D. thesis. Stanford University, Stanford, Calif.
9. **Girard, S., T. Couderc, J. Destombes, D. Thiesson, F. Delpeyroux, and B. Blondel.** 1999. Poliovirus induces apoptosis in the mouse central nervous system. J. Virol. **73:**6066–6072.
10. **Gustafsson, C., S. Govindarajan, and J. Minshull.** 2004. Codon bias and heterologous protein expression. Trends Biotechnol. **22:**346–353.
11. **He, Y., V. D. Bowman, S. Mueller, C. M. Bator, J. Bella, X. Peng, T. S. Baker, E. Wimmer, R. J. Kuhn, and M. G. Rossmann.** 2000. Interaction of the poliovirus receptor with poliovirus. Proc. Natl. Acad. Sci. USA **97:**79–84.
12. **Hogle, J. M.** 2002. Poliovirus cell entry: common structural themes in viral cell entry pathways. Annu. Rev. Microbiol. **56:**677–702.
13. **Holland, J. J., E. Domingo, J. C. de la Torre, and D. A. Steinhauer.** 1990. Mutation frequencies at defined single codon sites in vesicular stomatitis virus and poliovirus can be increased only slightly by chemical mutagenesis. J. Virol. **64:**3960–3962.
14. **Hsiao, L. L., F. Dangond, T. Yoshida, R. Hong, R. V. Jensen, J. Misra, W. Dillon, K. F. Lee, K. E. Clark, P. Haverty, Z. Weng, G. L. Mutter, M. P. Frosch, M. E. Macdonald, E. L. Milford, C. P. Crum, R. Bueno, R. E. Pratt, M. Mahadevappa, J. A. Warrington, G. Stephanopoulos, and S. R. Gullans.** 2001. A compendium of gene expression in normal human tissues. Physiol. Genomics **7:**97–104.
15. **Johansen, L. K., and C. D. Morrow.** 2000. The RNA encompassing the internal ribosome entry site in the poliovirus 5′ nontranslated region enhances the encapsidation of genomic RNA. Virology **273:**391–399.
16. **Joklik, W., and J. Darnell.** 1961. The adsorption and early fate of purified poliovirus in HeLa cells. Virology **13:**439–447.
17. **Kaplan, G., and V. R. Racaniello.** 1988. Construction and characterization of poliovirus subgenomic replicons. J. Virol. **62:**1687–1696.
18. **Koike, S., C. Taya, T. Kurata, S. Abe, I. Ise, H. Yonekawa, and A. Nomoto.** 1991. Transgenic mice susceptible to poliovirus. Proc. Natl. Acad. Sci. USA **88:**951–955.
19. **Molla, A., A. V. Paul, and E. Wimmer.** 1991. Cell-free, de novo synthesis of poliovirus. Science **254:**1647–1651.
20. **Murdin, A. D., and E. Wimmer.** 1989. Construction of a poliovirus type 1/type 2 antigenic hybrid by manipulation of neutralization antigenic site II. J. Virol. **63:**5251–5257.
21. **Neznanov, N., K. M. Chumakov, L. Neznanova, A. Almasan, A. K. Banerjee, and A. V. Gudkov.** 2005. Proteolytic cleavage of the p65-RelA subunit of NF-kappaB during poliovirus infection. J. Biol. Chem. **280:**24153–24158.
22. **Paul, A. V., J. A. Mugavero, A. Molla, and E. Wimmer.** 1998. Internal ribosomal entry site scanning of the poliovirus polyprotein: implications for proteolytic processing. Virology **250:**241–253.
23. **Pfister, T., and E. Wimmer.** 1999. Characterization of the nucleoside triphosphatase activity of poliovirus protein 2C reveals a mechanism by which guanidine inhibits poliovirus replication. J. Biol. Chem. **274:**6992–7001.
24. **Plotkin, J. B., H. Robins, and A. J. Levine.** 2004. Tissue-specific codon usage and the expression of human genes. Proc. Natl. Acad. Sci. USA **101:**12588–12591.
25. **Reed, L. J., and M. Muench.** 1938. A simple method for estimating fifty percent endpoints. Am. J. Hyg. **27:**493–497.
26. **Rothberg, E.** 1985. wmatch: a C program to solve maximum-weight matching. [Online.] http://elib.zib.de/pub/Packages/mathprog/matching/weighted.
27. **Rueckert, R. R.** 1985. Picornaviruses and their replication, p. 705–738. *In* B. N. Fields, D. M. Knipe, R. M. Chanock, J. L. Melnick, B. Roizman, and R. E. Shope (ed.), Fields virology, vol. 1. Raven Press, New York, N.Y.
28. **Sánchez, G., A. Bosch, and R. M. Pinto.** 2003. Genome variability and capsid structural constraints of hepatitis A virus. J. Virol. **77:**452–459.
29. **Schwerdt, C., and J. Fogh.** 1957. The ratio of physical particles per infectious unit observed for poliomyelitis viruses. Virology **4:**41–52.
30. **Svitkin, Y. V., G. A. Alpatova, G. A. Lipskaya, S. V. Maslova, V. I. Agol, O. Kew, K. Meerovitch, and N. Sonenberg.** 1993. Towards development of an in vitro translation test for poliovirus neurovirulence. Dev. Biol. Stand. **78:**27–32.
31. **Svitkin, Y. V., S. V. Maslova, and V. I. Agol.** 1985. The genomes of attenuated and virulent poliovirus strains differ in their in vitro translation efficiencies. Virology **147:**243–252.
32. **Tolskaya, E. A., L. I. Romanova, M. S. Kolesnikova, T. A. Ivannikova, E. A. Smirnova, N. T. Raikhlin, and V. I. Agol.** 1995. Apoptosis-inducing and apoptosis-preventing functions of poliovirus. J. Virol. **69:**1181–1189.
33. **van der Werf, S., J. Bradley, E. Wimmer, F. W. Studier, and J. J. Dunn.** 1986. Synthesis of infectious poliovirus RNA by purified T7 RNA polymerase. Proc. Natl. Acad. Sci. USA **78:**2330–2334.
34. **Wimmer, E., C. U. T. Hellen, and X. M. Cao.** 1993. Genetics of poliovirus. Annu. Rev. Genet. **27:**353–436.
35. **Zhao, W. D., and E. Wimmer.** 2001. Genetic analysis of a poliovirus/hepatitis C virus chimera: new structure for domain II of the internal ribosomal entry site of hepatitis C virus. J. Virol. **75:**3719–3730.
36. **Zolotukhin, S., M. Potter, W. W. Hauswirth, J. Guy, and N. Muzyczka.** 1996. A "humanized" green fluorescent protein cDNA adapted for high-level expression in mammalian cells. J. Virol. **70:**4646–4654.